Regulation of *bicoid* mRNA throughout oogenesis and early embryogenesis impacts protein gradient formation

T. Athilingam[1,+], E.L. Wilby[2,+], P. Bensidoun[3], A. Trullo[3], M. Verbrugghe[3], M. Lagha[3], T.E. Saunders[1,*], T.T. Weil[2,*]

[1] Warwick Medical School, University of Warwick, Coventry, CV4 7AL, United Kingdom
[2] Department of Zoology, University of Cambridge, Cambridge, CB2 3EJ, United Kingdom
[3] Institut de Génétique Moléculaire de Montpellier, Univ Montpellier, CNRS, Montpellier, France.

[+] Equal contribution, listed alphabetically
[*] For correspondence: timothy.saunders@warwick.ac.uk, tw419@cam.ac.uk

Abstract

The transcription factor Bicoid (Bcd) establishes patterning in the early *Drosophila* blastocyst through its graded concentration along the anterior-posterior (AP) axis. *bcd* mRNA is maternally deposited during oogenesis, yet precisely when and where *bcd* mRNA is translated remains an open problem. Here, we take advantage of the SunTag reporter system to quantitatively examine the spatiotemporal profile of *bcd* mRNA translation *in vivo*. We demonstrate that Processing body (P body) localisation in the oocyte suppresses premature *bcd* mRNA translation. Upon egg laying, *bcd* mRNA disassociates from P bodies and translation is observed exclusively in the anterior pole of the embryo. Accompanying nuclear migration to the embryo cortex at nuclear cycle (n.c.) 9, *bcd* mRNA relocates to the apical domain of the nuclear environment and translation continues near the embryo surface. In n.c. 14, *bcd* mRNA localises to newly formed P bodies and further translation is not detected. We use these observations to build a modified source-diffusion-degradation model of Bcd gradient formation that leads to an exponential gradient by n.c. 12 and is consistent with other experimental measurements of Bcd dynamics. Consequently, we see that the spatiotemporal dynamics of *bcd* mRNA translation are highly regulated throughout oogenesis and early embryo development.

Key words

Translation, morphogen, P bodies, mRNA regulation, body-axis patterning

Introduction

The concept of signalling molecules, coined morphogens, that instruct spatial patterning through their spatially inhomogeneous concentration within developing systems was proposed by Turing (1). Downstream target genes respond in a concentration-dependent manner to the morphogen concentration (2). Bcd, a transcription factor present in the early *Drosophila* blastocyst, was the first identified morphogen gradient (3). A concentration gradient of Bcd extends along the AP axis from highest in the anterior pole of the embryo to around 70% embryo length, with the expression profiles of downstream target genes such as *hunchback* dependent on the local Bcd concentration (4-6).

Soon after its discovery, the Synthesis, Diffusion, Degradation (SDD) model was proposed as a mechanism for Bcd gradient formation (3, 7). This model assumed localised production of Bcd in the anterior pole, followed by diffusion through the embryo and subsequent degradation. Such a model predicted an exponentially decaying concentration profile in steady state, as observed *in vivo* (7-9). Yet, there are multiple mechanisms that can generate exponentially decaying morphogen profiles (10, 11). Alternatives to the SDD model include: (i) local production (*i.e.* translation) of Bcd, by the *bcd* mRNA (henceforth referred to by *bcd*) being spatially distributed along the embryo (12); (ii) early translation of *bcd* in the oocyte, enabling quick spread of the morphogen prior to patterning in later nuclear cycles (13); and (iii) nuclear dilution, which does not require protein degradation (14). These models make distinct predictions for when and where *bcd* is translated, yet they can all form exponential-like concentration gradients in appropriate parameter regimes at relevant time scales for patterning (15-17).

Localised *bcd* is first observed in mid-stage oocytes and shows continued enrichment in late oogenesis (18-20). As the egg matures, *bcd* transitions from continued active transport to stable anchoring at the anterior cortex (20, 21). After oogenesis, all *bcd* that is required for anterior patterning in the embryo is localised tightly to the anterior cortex of the mature oocyte (Figure 1A) (18-21). There is no current biochemical evidence for *bcd* translation before egg activation (22-24), a conserved process for a suite of changes in the egg, including re-initiation of meiosis, a change in the translational landscape, and reconfiguration of the cytoskeleton, as the mature egg enters the oviduct prior to fertilisation (25). Translational repression of *bcd* in the oocyte is thought to be regulated by association with a cytoplasmic biomolecular condensate (26, 27).

Research into condensate function, composition, and physical properties, has largely focused on single cell models and *in vitro* systems (28-32). These data have provided an excellent

foundation for exploring translational regulation via condensates in multicellular organisms. The ability to manipulate condensates genetically and physically in *Drosophila* has recently been shown to be insightful for deciphering the biological relevance of RNP granules in a developmental context (33-37).

The use of phase-separated droplets as a mechanism for regulating localised translation in the *Drosophila* oocyte is well illustrated by work on the oocyte posterior. Visualisation of *nanos* mRNA translation reveals that germ granules can be translation sites or repression dependent on localisation (36). The germ-line determinant *oskar* (*osk*) mRNA associates with "solid-like" condensates where its unique secondary structure is required to maintain *osk* RNA inside the condensates, where it is translationally repressed (33).

A similar model of RNA regulation via association with biomolecular condensates had previously been proposed for *bcd* (26, 27). Once localised to the anterior, *bcd* is sequestered in the core of P bodies away from ribosomes (26). P bodies are a conserved condensate that, dependent on the cellular context, have been implicated in the storage and degradation of mRNA (28, 38). A range of proteins involved in mRNA regulation is found to be enriched in P bodies, including DEAD-box family RNA helicase Maternal Effect at 31B (Me31B), which has homologies in other species (DDX6 -humans , Dhh1 - *S.cerevisiae*, Xp54 - *Xenopus*, Cgh-1 - *C.elegans*) (26, 39). Previous work has shown that Me31B functions both in repression and clearance of maternal transcripts in early embryogenesis (40).

With regards to formation of the Bcd morphogen gradient, previous work has typically either focused on the regulation of *bcd* during oogenesis (26, 41-43) or on the dynamics of Bcd protein post-translation (7, 10, 17, 44, 45). Yet, to gain a more complete understanding of how the Bcd gradient forms requires integrating these two approaches. Here, we utilised the imaging-based SunTag/scFv reporter system (46-53), to quantitatively assay *bcd* translation in *Drosophila* oocytes and embryos. In the oocyte, we demonstrate that P body localisation of *bcd* inhibits translation and dissociation from P bodies results in *bcd* translation. Upon egg activation, *bcd* mRNAs are released from the P bodies and we observed rapid onset of *bcd* translation, strictly limited to the anterior pole of the embryo. Following nuclear migration to the embryo outer membrane (n.c. 9), *bcd* localisation became more apically positioned, with a corresponding shift in the location of translation. We saw a decrease in *bcd* translation in n.c. 11 onwards, consistent with observations from assaying the protein levels (54). Finally, we demonstrate that a modified SDD model of Bcd gradient formation, where the source of Bcd changes in both space and time based on experimental observations, is consistent with the observed *bcd* translation and the Bcd protein gradient.

Results

bcd mRNA associated with P bodies in the oocyte until egg activation

Previous work analysed the relationship between *bcd* and P body proteins during oogenesis (26, 27), and postulated that *bcd* localisation to P bodies is important for translational regulation of the mRNA. To confirm if this relationship is maintained through the mid and late stages of oogenesis, we simultaneously imaged a standard P body marker, Me31B, and *bcd* (Figure 1B-C). We performed single molecule FISH (smFISH) for *bcd* in tissue that expresses endogenously tagged Me31B, which is subsequently "boosted" with an anti-GFP-nanobody conjugated to a photostable dye (Methods).

During the transition from mature oocyte to activated egg, P bodies disassembled (26, 27, 55) and Me31B became evenly distributed in the cytoplasm. *bcd* similarly dispersed and lost its tight association with the anterior cortex (Figure 1D-F). The distribution of *bcd* was maintained in the early embryo when 'embryonic' P bodies appeared to reassemble with unique characteristics compared to those in the oocyte (Figure 1D-F). Based on these results and previous observations (26, 27), we hypothesised that the loss of colocalisation between *bcd* and P bodies correlates with *bcd* translation.

bcd translation only begins after egg activation

To test when and where *bcd* is translated in the oocyte and embryo, we generated a *SunTag-bcd* transgene, containing an array of 32X SunTag repeats, referred to here as *bcdSun32* (Figure S1, Methods). Prior to exploring the capacity of *bcd* to be translated in oocytes, we first validated our reporter in fixed early embryos. To this end, we performed immuno-FISH, labelling *bcdSun32* as well as the SunTag peptide, recognised by an anti-GCN4 antibody. We also performed this validation in the presence of the fluorescent detector, the single-chain antibody scFV, which is genetically encoded and maternally provided (*nos-scFv-MSGFP2*) (56).

After validating our *bcdSun32* reporter by showing co-localisation between the RNA and protein in early embryos (Figure S1), we genetically expressed *bcdSun32* in oocytes. We observed no translation in any region of stage 9 or 14 oocytes (Figure 2A-B), consistent with predictions based on previous observations of *bcd* localisation to P bodies (26, 27). However, after egg activation, *bcd* translation occurred rapidly and continued after egg laying (22, 57) (Figure 2C). Consistent with previous observations of *bcd* localisation (3), we only observed translation in the anterior of the activated egg and early embryo (Figure 2C).

145 To test whether co-localisation of *bcd* with P bodies was necessary for its translational
146 repression, we first sought to maintain the relationship between *bcd* and P bodies through egg
147 activation (Figure 2D-G). We utilised a pharmacological reagent known to disrupt the calcium
148 wave that transverses the activated egg while other phenotypic markers of egg activation are
149 observed (58). Incubation of oocytes with NS8593 caused a failure to disperse P bodies during
150 *ex vivo* egg activation (Figure 2D). smFISH on NS8593 treated activated oocytes showed that
151 *bcd* association with P bodies was maintained in large particles close to the anterior margin
152 (Figure 2D,F). Consistent with our predictions, we did not observe translation of *bcdSun32* in
153 NS8593 treated activated oocytes (Figure 2E,G). Together, this suggests that P bodies act as
154 a physical barrier that maintains *bcd* transcripts within a translation-free environment in the
155 oocyte.
156
157 **Premature release of *bcd* mRNA results in ectopic translation**
158 Altering the physical state of a condensate can impact its ability to store mRNA (27, 33, 59).
159 To further test if *bcd* storage in P bodies is required for translational repression, we monitored
160 mRNA association with P bodies under different chemical treatments known to disrupt
161 condensate integrity (60-62). The addition of Hexanediol or NaCl to mature oocytes resulted
162 in *bcd* detected outside of P bodies (Figure 3A-C). Following treatment of mature oocytes with
163 these chemicals, we observed BcdSun32 protein in the oocyte anterior (Figure 3D-E). To
164 ensure that the chemical treatments did not inadvertently activate the mature eggs, resulting
165 in translation, we assayed for egg activation (57). Chemically treated eggs did not survive the
166 activation test (63), thus confirming that the storage in P bodies is important to maintain *bcd*
167 translational repression.
168
169 To further challenge this model, we utilised mutations in *Drosophila* Endosulfine (Endos) (64),
170 which resulted in a similar change in condensate phenotype at egg maturation as those
171 observed with chemical treatments (Figure 3F). This temporal effect was consistent with the
172 known roles of Endos, part of the conserved phosphoprotein α-endosulfine (ENSA) family,
173 which has been previously described as the master regulator of oocyte maturation in
174 *Drosophila* (64, 65). Endos mutant oocytes showed a loss of colocalisation between *bcd* and
175 P bodies, concurrent with the transition to a less viscous P body state at oocyte maturation
176 (Figure 3F-G, Figure S2). Particle size and positional analysis showed *bcd* RNPs undergoing
177 a premature transition to an embryo distribution (Figure 3H-I). Due to genetic and antibody
178 constraints, we are unable to test for translation of *bcd* in the *Endos* mutant by
179 immunofluorescence or Western blot. However, based on our SunTag and smFISH data
180 presented here, we posit that *bcd* observed in this diffuse distribution outside of P bodies
181 would be translationally active (Figure 3F-H).

182 ***bcd* translation is spatially restricted during early *Drosophila* embryogenesis**
183 We next asked when and where *bcd* is translated in the embryo. Specifically, is *bcd* translation
184 restricted to the anterior pole and when is the maximum translation rate reached?
185
186 We considered that the size of *bcdSun*32 may impede mRNA biogenesis and the function of
187 SunTag-bcd as a transcription factor. Therefore, we generated a second transgene with fewer
188 SunTag repeats (10x), referred to as *bcdSun10* (Figure S3). *bcdSun10* rescued the bcd^{E1} null
189 mutant, suggesting that the tag does not significantly impact function (Figure S3). We
190 performed Immuno-smFISH on *bcdSun10* and *bcd* in n.c. 4 (Figure 4A), to explore the spatial
191 pattern of Bcd protein production. We saw a strong correlation between *bcd* and sites of
192 translation in the anterior (Figure 4B), with no observable translation greater than 75μm from
193 the anterior pole. The Bicoid gradient has small but reproducible differences between dorsal
194 and ventral surfaces (4). Consistent with this, we saw that the translation profile differed from
195 dorsal to ventral sides (Figure 4A lower panels) as the extent of *bcd* spread is uneven.
196
197 We next quantified the number of translation events in n.c. 4 (Methods, Figure S4) in different
198 regions. We found that in the anterior region of the embryo (<50 μm from the pole), above
199 90% of overall *bcd* particles are engaged in translation (Figure 4C-C'). Over 98% of all
200 observed translation events occurred within 50 μm of the anterior pole, with almost none seen
201 beyond 100 μm.
202
203 In the cross-sectional view, *bcd* is distributed steeply along the apical-basal axis with the
204 majority of *bcd* localised to within 10-12 μm from the embryo's surface (Figure S5A-B). We do
205 not observe any variation with depth from the surface in the rate of *bcd* translation (Figure
206 S5C-D). Overall, we did not see evidence for spatial differences in the translation efficacy. We
207 conclude that during early embryogenesis before nuclear migration to the cortex, *bcd*
208 translation is strictly localised to the anterior domain (<50 μm from the anterior pole).
209
210 **Spatiotemporal pattern of *bcd* translation**
211 We analysed 3D image stacks at different stages of embryo development from n.c.4 to late
212 n.c. 14. In the early embryo (<n.c.9), *bcd* translation occurred in a broad strip near the embryo
213 cortex in the anterior (Figure 5A). There was sustained translation of *bcd.* After nuclear
214 migration to the periphery in n.c. 9, we observed a gradual decrease in translation events
215 (Figure 5A-B). By late n.c. 14, translation events were barely detected (Figure 5A-B).
216
217 mRNA translation can depend on location within the cytoplasm. For example, *twist* mRNA
218 residing apical to the nuclei had lower translation compared to basal mRNAs (51). Before

219 cortical migration of nuclei, *bcd* translation did not show variation from the surface to up to 10
220 µm from the surface (Figure S5C-D). Does the domain of *bcd* translation vary upon nuclear
221 migration to the periphery? Interestingly, we observed that after the cortical migration, the
222 number of *bcd* translation events showed differences with respect to localisation above and
223 below the nuclei (Figure 5C). Upon cortical migration, we also noticed that *bcd* localisation in
224 the anterior pole became more dispersed (Figure S6). The interphase nuclei and their
225 subsequent mitotic divisions appeared to displace *bcd* towards the apical surface (Figure S6A-
226 B).
227
228 We can directly test different models of Bcd protein production (3, 10, 12, 54) and how this
229 impacts the formation of the Bcd morphogen gradient. After translation, a gradient of Bcd
230 needs to form. We compared the concentration profiles between *bcd* and the protein
231 distribution in our *bcdSun10* line. In the anterior pole, in the cytoplasm, we observed
232 localisation of *bcd* with our SunTag reporter (Figure S7). The nuclear profile of Bcd protein
233 extended further than the *bcd* mRNA gradient (Figure S7A'), consistent with an SDD-like
234 model of gradient formation. Further, >98% of all translation events happen within 50µm of
235 the anterior pole (n=3 embryos) regardless of nuclear cycle. The efficiency of translation could
236 vary at different positions in the embryo. We quantified the intensity of translation events along
237 the anterior-posterior axis, but did not observe any clear changes in translation intensity at
238 individual locations (Figure 5D-E). Together, these results suggest that a long-ranged gradient
239 of Bcd production does not occur at any time through n.c. 4-14.
240
241 Overall, we see a steady shift in the domain of *bcd* translation, which correlates with nuclei
242 movements during the blastocyst stage. However, this shift does not result in more dispersed
243 *bcd* translation along the AP axis. There is a significant reduction in translation, especially
244 from n.c. 13 onwards.
245
246 ***bcd* mRNA degradation in n.c. 14 (stage 5) embryos**
247 After the translation decrease, *bcd* is completely degraded during n.c. 14 (Figure 6A-C) (12,
248 66). The colocalisation of mRNAs with embryonic P bodies is correlated with degradation (67-
249 69). To test whether *bcd* was being targeted for degradation in embryonic P bodies, we
250 observed and analysed *bcd* and Me31B before, during, and after n.c. 14 (Figure 6A-C).
251 smFISH revealed an even distribution of *bcd* on the apical and basal side of the nuclei, which
252 did not colocalise with P bodies prior to n.c. 14 (Figure 6A).
253
254 At the start of n.c. 14, *bcd* was localised to the apical side of the nuclei (12), where we
255 observed colocalisation with embryonic P bodies that were also enriched on the apical side

(Figure 6B,D-E). As the embryo transitioned into gastrulation, we observed a significant loss of *bcd* while embryonic P bodies remained (Figure 6C-D,F). Together, this supports a model whereby rapidly degrading mRNAs present in the embryo are localised to embryonic condensates for degradation as the embryo transitions to zygotic control (67-69).

Adapted SDD model of Bcd protein gradient formation

Formation of the Bcd morphogen gradient has been extensively modelled (11, 15, 70). Yet, previous models typically considered the rate of Bcd production to be constant throughout early embryogenesis. We next asked whether accounting for the spatiotemporal pattern of *bcd* translation within the SDD model was consistent with the observed Bcd gradient.

We considered the concentrations of *bcd* mRNA (denoted by *[bcd]*) and the protein *[Bcd],* where the concentrations are functions of both space and time, within a modified SDD model (Figure 7A):

$$\frac{\partial[bcd]}{\partial t} = -\alpha(t)[bcd] \qquad \text{(Eq. 1a)}$$

$$\frac{\partial[Bcd]}{\partial t} = \frac{\partial}{\partial x}\left[D(x)\cdot\frac{\partial[Bcd]}{\partial x}\right] - \mu[Bcd] + \beta[bcd] \qquad \text{(Eq.1b)}$$

We defined time t =0 to denote egg activation. The initial conditions for [*bcd]* and [Bcd] were given by

$$[bcd](t=0,x) = f(x) \qquad \text{(Eq. 2a)}$$

$$[Bcd](t=0,x) = 0 \qquad \text{(Eq. 2b)}$$

bcd was localised in the anterior pole with a form denoted by *f(x)*, (Eq. 2a), shown in Figure 7B(i). We incorporated a delay initially in translation to account for egg activation (Figure 7B(ii)). The rate of *bcd* degradation $\alpha(t)$ increased markedly in n.c. 14 (Figure 7B(iii)). It was recently observed that the effective diffusivity of Bcd varies between the anterior and posterior pole (45). We included this through spatial variation in the diffusion coefficient *D(x)* (Figure 7B(iv)). We assumed that the rate of *bcd* translation (β) (after egg activation) and Bcd degradation (μ) remained constant. The degradation rate for Bcd has been measured previously based on protein lifetime measurements (10).

Our modified one-dimensional SDD model generated an exponential-like gradient of Bcd in n.c. 13 (Figure 7C-C'). We emphasise that all the parameters in this model are constrained by experimental measurement, except for β, so it is not over parameterised (Table S6). We found a decay length of around 85-95 μm, consistent with experimental measurements (7, 10, 54). By including more realistic *bcd* translation within the model, the overall behaviour of the Bcd

292 protein gradient (Figure 7D-D') is consistent with previous observations (54) and our
293 quantification here.
294
295 **Discussion**
296 We have provided a quantitative dissection of when and where *bcd* is translated in early
297 *Drosophila* development. Translation is restricted to post egg laying by localisation within P
298 bodies in the oocyte. Translation occurs in the anterior pole of the embryo and undergoes a
299 marked decrease after n.c. 11. Around this time, *bcd* becomes localised to the apical domain
300 and is rapidly degraded, especially in n.c. 14. This rapid degradation of *bcd* correlates with its
301 localisation to P bodies during cellularisation. We show that these observations, in concert
302 with recent quantification of Bcd dynamics (45), are consistent with a modified SDD model of
303 gradient formation.
304
305 In early embryos, Bcd protein is only observed in the anterior pole. This corresponds tightly
306 with the pattern of *bcd* translation; no significant translation was observed >50μm from the
307 embryo anterior. These results argue against *bcd* translation in the oocyte, resulting in long-
308 ranged protein dispersal. Another model has proposed that *bcd* is distributed through the
309 embryo and hence can generate a long-ranged gradient of Bcd without the need for diffusive
310 transport (12, 71, 72). However, we observe the vast majority of translation events only
311 occurred within 50 μm of the embryo anterior pole. Consistent with previous reports (54), we
312 posit this is due to *bcd* localisation in the anterior region (<100μm), rather than there being
313 regulation impacting *bcd* translation in more posterior regions. Consequently, any graded form
314 of *bcd* translation appears to be largely localised to the anterior; this suggests that a long-
315 ranged *bcd* translation gradient does not determine the Bcd protein gradient extent.
316
317 We noticed distinct differences in the apical-basal localisation of *bcd,* especially after nuclear
318 migration to the embryo cortex. This alteration in apical-basal distribution correlates with a
319 reduction in the observed *bcd* translation. However, whether the localisation of *bcd* impacts
320 its rate of translation remains to be tested further. The localisation of mRNAs within the
321 microenvironment defined by each nuclear domain can impact translation in n.c. 14 (51),
322 though whether a similar effect occurs earlier in development is unclear.
323
324 The rapid loss of *bcd* in n.c. 14 has been previously quantified (54) and here we discovered it
325 also correlates tightly with localisation to P bodies (Figure 6). What determines the model of
326 *bcd* degradation in n.c. 14? Is it due to global degradation of maternal mRNA or because of a
327 specific regulation of bcd mRNA (40)? Testing for *bcd* degradation is challenging. One method

is to use different smFISH probes for the 5' and 3' UTRs and use differences in the spectral signal to infer degradation (69, 73). However, the *bcd* 5' UTR is very short, and we were unable to make effective smFISH probes. One possible alternative is to target the *bcd* instability element (BIE). This regulates degradation of *bcd* (66) and is located within the more accessible 3' UTR.

It will be interesting to probe further the functional effects of differences in P bodies between the oocyte and during cellularisation. The P bodies appear to switch function, from shielding *bcd* from translation to enhancing degradation. Prior to cellularisation, we found that Me31B condensates were insensitive to cycloheximide. However, after cellularisation begins, they become sensitised to cycloheximide (74), suggesting a change in their structure. Relatedly, due to the conserved nature and wide-ranging downstream effects, it is intriguing to consider the possibility that Endos is a condensate regulator both within *Drosophila* eggs as well as more generally.

Over 40 years of work span from the original proposition of the SDD model for Bcd gradient formation. Here, we quantitatively assay the production of Bcd *in vivo*, which is arguably the last piece required to understand Bcd gradient formation. We see that the SDD model as originally proposed was too simple, but with suitable modifications – *e.g.,* spatially varying diffusion and temporally altering translation – it can explain the formation of the Bcd gradient.

Contributions:

Project conception: ML, TES, TTW. Experimental design: TA, ELW, ML, TES, TTW. Experiments: TA and ELW with support from PB, MV and ML. Analysis: TA and ELW, with support from AT, TES and TTW. Modelling: TES. Writing: TA, ML, TES, ELW, TTW with all authors contributing to final version. Funding acquisition: ML, TES, TTW.

Acknowledgements

We are very grateful to members of the Lagha, Saunders and Weil labs for support and comments on the project. We thank Jeremy Dufourt for advice on initial strategy for using Suntag with Bicoid and sharing plasmids (51). ML funding: ERC lightRNA2Prot and CNRS. TES thanks core funding from the Mechanobiology Institute, Singapore and startup funding from Warwick Medical School. TTW thanks the Wellcome Trust Institutional Strategic Support Fund, University of Cambridge (grant number 097814) and Biotechnology and Biological Sciences Research Council Doctoral Training Partnerships studentship (ELW). ML acknowledges the Montpellier Resources Imaging facility (France-BioImaging)

364 and the *Drosophila* facility (Biocampus). The funders had no role in study design, data
365 collection and analysis, decision to publish, or preparation of the manuscript.
366
367 **Methods**
368 **Generation of SunTag *bcd* transgenic fly lines**
369 *bcdSun32* was generated by replacing N-terminal eGFP of eGFP:Bcd-pCaSpeR4 construct
370 (kindly gifted by Thomas Gregor (7)) by 32xSunTag repeats (kindly gifted by Mounia Lagha
371 (51)). The 32xSunTag fragments are flanked by NheI and SpeI restriction sites at their N and
372 C-terminal ends respectively by PCR, and then ligated into the eGFP:Bcd construct, replacing
373 eGFP. Likewise, the first 10xSunTag repeats of 32xSunTag were ligated in the same way to
374 generate *bcdSun10* construct (Figure S1A). Both Bcd SunTag constructs from the donor
375 pCaSpeR4 construct were recombined into w+attB construct (addgene 30326) and flies were
376 generated by phiC31 recombination into attP40 site of chromosome 2. The injection and
377 generation of fly lines were done by BestGene Inc. USA.
378
379 The *bcdSun10* fly lines were crossed to the *bcd* null allele mutant, bcd^{E1}. *bcdSun10*;bcd^{E1} fly
380 lines were viable, suggesting our construct can, at least partially, complement the function of
381 endogenous Bcd. smFISH was carried out to test if *bcdSun10*;bcd^{E1} effectively replaced the
382 function of endogenous Bcd in the blastoderm. Stellaris smFISH probes with distinct
383 fluorophores were used for SunTag and *bcd* coding regions of the *bcdSun10* mRNA. This
384 enabled us to confirm that the only contribution of maternal *bcd* mRNA was from our *bcdSun10*
385 in the bcd^{E1} background (Figure S2). Colocalisation analysis in the early blastoderm revealed
386 ~90% of the mRNA were accounted for *bcdSun10* (Figure S2B). Further, the immunostaining
387 of the blastoderm embryos with anti-GCN4 antibody revealed the translocation of the
388 *bcdSun10* into the nuclei, unlike *bcdSun32*, eventually forming an anterior posterior gradient
389 similar to endogenous Bcd (Figure S2C-E).
390
391 **Preparation of oocytes**
392 Twenty female flies and ten male flies of the correct genotype were transferred into a vial
393 containing fly food supplemented with yeast and were incubated at 25°C for forty-eight hours
394 before dissection (75).
395
396 **Oocyte dissection**
397 Fattened or aged female flies were anaesthetised, and the posterior tip of the abdomen was
398 removed using a set of fine forceps. The ovaries were then removed from the open posterior
399 end by squeezing the abdomen (75).
400

401 **Fly husbandry and preparation of embryos**

402 Fly stocks were maintained at 21°C in vials that contained standard cornmeal starch agar fly
403 food. To collect flies for experimentation or for genetic crosses, twenty females (virgin females
404 were used for genetic crosses) and ten males were transferred into a plastic bottle containing
405 yeasted cornmeal starch agar fly food at 25°C. Either virgin females or males from this
406 generation were used for additional genetic crosses, or females younger than 10 days old
407 were selected for experimentation. Collected embryos were dechorionated in 50% bleach for
408 2 minutes before excess bleach was removed with distilled water.

409

410 **Chemical and pharmacological treatments of oocytes**

411 Hexanediol and sodium chloride: Dissected oocytes were incubated for 20 minutes in 5% 1,6-
412 HD, 5% 2,5-HD, or 400 mM NaCl before immediate fixation. As controls, dissected oocytes
413 were incubated in PBS or SIM for equal amounts of time before fixation.

414

415 *in vitro* activation of stage 14 oocytes (fixed): Dissected stage 14 oocytes were incubated in
416 activation buffer (AB), for 30 minutes at room temperature. Activated oocytes were incubated
417 in SIM for 0-30 minutes. To ensure that only activated oocytes were visualised, oocytes were
418 treated with 50% bleach for two minutes. The activated oocytes were then fixed using the
419 embryo fixation method. As a control, oocytes were incubated in SIM for the same time period.

420

421 Drugs that inhibit the calcium wave: Dissected stage 14 oocytes were incubated in SIM that
422 contained NS8593 for 30 minutes. The oocytes were then activated in vitro following the same
423 steps as above, with all solutions containing the pre-incubation drug. As a control, oocytes
424 were incubated in SIM (with no AB step) with the drug. Additionally, oocytes were incubated
425 in SIM, followed by AB, followed by SIM with a 1:1000 dilution of either DMSO or ethanol.

426

427 **Fixation**

428 Oocytes were incubated 1 ml of 4% paraformaldehyde for 15 minutes before immediate
429 washing with 0.1% PBST (76). 10-20 pairs of ovaries were dissected and transferred to room-
430 temperature Schneider's Insect Medium (SIM). Ovaries were teased apart using dissecting
431 probes until single ovarioles and oocytes were released.

432

433 Embryos were transferred into an Eppendorf tube that contains equal parts paraformaldehyde
434 and heptane for 15-30 minutes, depending on the probes or antibodies used, before the
435 paraformaldehyde phase was removed and replaced with 100% methanol. The sample was
436 then shaken vigorously before all the solution was removed. Embryos were then rinsed with
437 methanol and/or ethanol before being washed in 0.1% PBST (76).

438

439 **Single molecule fluorescence *in situ* hybridisation (smFISH)**

440 Probe design: Custom 20 nucleotide Stellaris FISH Probes were designed against the 3' UTR
441 of *bcd,* coding region of *bcd*, and 32x SunTag by utilising the Stellaris RNA FISH Probe
442 Designer and were the same as designed in (65) (Biosearch Technologies, Inc
443 - www.biosearchtech.com/stellarisdesigner). 32x SunTag and *bcd* 3'UTR Probes were
444 labelled with Quasar 570 and endogenous *bcd* is labelled with Quasar 670 were ordered for
445 smFISH from Biosearch Technologies, Inc.

446

447 Buffers: Wash buffer was created by mixing the commercially available 'Wash Buffer A', de-
448 ionised formamide and nuclease free water in a 2:1:7 ratio or was made using 2% sodium
449 citrate buffer (SSC)+10% formamide. Hybridisation Buffer was created by mixing 'Stellaris
450 Hybridisation Buffer' with de-ionised formamide in a 9:1 ratio.

451

452 Hybridisation: The hybridisation protocol was adapted from (51, 54). Briefly, fixed oocytes or
453 embryos were permeabilised with 0.2% triton X-100 and washed in PBST. When necessary,
454 embryos were blocked in PBST+RNase inhibitor+0.5% ultrapure BSA for 45 mins, before
455 being washed in a 'wash buffer' solution. The samples were then pre-incubated in
456 hybridisation buffer for two hours at 37°C. The hybridisation buffer was removed and replaced
457 by the hybridisation buffer with smFISH probes for overnight incubation at 37°C, when using
458 anti-GCN4 antibodies in conjunction with smFISH, primary antibodies were incubated
459 overnight in the hybridisation buffer (56). The samples were then washed in hybridisation
460 buffer before repeated washes in prewarmed wash buffer, when using anti-GCN4 antibodies
461 in conjunction with smFISH, secondary antibodies were incubated with the final wash buffer
462 wash, before being washed in 2X SSC. Finally, all samples were washed multiple times in
463 0.1% PBST.

464

465 Immunostaining: Nanobody labelling on oocytes or embryos, samples were blocked in a 4%
466 BSA solution and then incubated with nanobodies, either GFP booster or RFP booster, in
467 0.1% PBST for one hour at room temperature. For anti-GCN4 immunostaining not in
468 conjunction with smFISH, samples were incubated for two hours with the primary antibody,
469 followed by washing with 0.1% PBST and incubation with the secondary antibody for two
470 hours. After incubation, all samples were washed with 0.1% PBST.

471

472 Washed samples were transferred to a microscope slide and positioned using a dissecting
473 probe. Excess PBST was removed before a single drop of Slowfade Diamond with DAPI or
474 Prolong Diamond with antifade was added to the sample. A 22 x 22 mm coverslip was lowered

475 onto the sample, and the coverslip was sealed with nail varnish and laid flat in the dark for 24
476 hours before imaging.
477
478 Imaging: All oocyte imaging was completed on an Olympus FV3000 inverted confocal
479 microscope. Embryo imaging was performed on Olympus FV3000 or Olympus Spinning Disc
480 systems. All images were taken using silicone oil 30x (0.95 NA) or 60x (1.4 NA) objectives. A
481 region of interest was placed around either a whole single oocyte or embryo (30x objective)
482 or a specific region of the oocyte or embryo (60x objective), Images were taken at a resolution
483 of 1024 by 1024, or 2048 by 2048 pixels. 405, 488, 561 and 640 nm lasers were used. Laser
484 power was adjusted to ensure that there was a full range of grey values and that the saturation
485 of pixels was limited.
486
487 The images for the quantification of *bcd* foci in the embryo and their colocalisation to
488 translating SunTag, were acquired on an Olympus FV3000 confocal microscope with the
489 following conditions: 60x magnification, 4x zoom, 2 line averaging, slice thickness of 0.4 µm.
490 The regions of high, moderate, and low dense *bcd* foci from the anterior domain and a very
491 low *bcd* region in the posterior were imaged for a total thickness of 10-15 µm.
492
493 Fixed Imaging: Optimised step-size Z-stacks of fixed egg and embryos were collected; all Z-
494 stacks were started at the cortex and extended 10-15 µm into the oocyte or embryo. For co-
495 localisation studies, smFISH, and SunTag translation assays, where maximum resolution was
496 imperative. Imaging parameters were optimised to improve resolution: 60 x objective used;
497 pinhole: 1 airy unit; scan speed – 400 Hz; 2x line averaging; 2048 by 2048 pixels; and
498 optimised Z-step (300 nm) (52).
499
500 **Image Analysis**
501 Translation quantification: High-resolution image stacks were segmented to identify specific
502 *bcd* foci. We used the trainable Weka segmentation plugin of ImageJ to train and classify the
503 *bcd* foci. A classifier model created from a single image slice was applied to the Z-stack, thus
504 classifying the *bcd* through the whole stack. The segmented particles were analysed using the
505 Fiji particle analysis plugin that provided information on the size, shape, intensity and counts
506 of all particles. The crowded particles that failed to segment properly, which was often the
507 case within highly dense *bcd* regions, were not considered. We also excluded foci with low
508 brightness. The segmented ROIs of *bcd* foci were applied to the anti-GCN4 channel. The
509 mean intensities from anti-GCN4 channel were background corrected, and the positive mean
510 values provided the number of colocalising SunTag to *bcd* particles *i.e.,* these particles were
511 translating *bcd* (Figure 4D). The plots were made in Graphpad Prism 8.0.

When automated methods were not accurate for detecting partial co-localisation (77), manual analyses were undertaken on images with only partial co-localisation. Images for both channels were thresholded, then an overlay of the threshold outline for channel one (*bcd*) was projected onto the channel two image (anti-GCN4). The number of particles in *bcd* channel that overlapped particles in anti-GCN4 channel was counted, and *vice versa*. To ensure that this partial co-localisation was not due to chance, images of one channel were inverted and the analysis was completed again.

Statistical Analysis

n numbers: 10 to 20 females or 30 embryos (biological repeats) were used for each experiment and a global overview of the experimental results was acquired by visualising 20-30 oocytes or 30 embryos for each experimental condition unless stated otherwise. A smaller number of representative oocytes were subjected to high resolution imaging and analysis as described above. The “n” used in figures represents independent oocyte or embryo samples.

All statistical analyses were performed in R. For all statistical analyses, asterisks represent the following n.s. not significant * $P<0.05$, ** $P<0.01$, *** $P<0.001$.

Continuous data: Tests for normality were completed before proceeding with the appropriate parametric or non-parametric test. For comparison between two groups, an unpaired student t-test (STT) or a Wilcoxon signed-rank test (WSRT) was used.

Categoric data: A χ^2 test (CST) or Fisher’s exact test (FET) was used to determine if there were significant differences between groups. This depended on sample size Fisher’s exact test is preferred for small sample sizes (<50).

538 **Fly lines**

Fly line & genotype	Source and identifier
Visualisation of proteins	
Me31B::GFP (Endogenous Tag)	(78) BDSC: 51530
Suntag-Bcd W; 32xSuntag-Bcd/ Cyo W;10xSunTag-Bcd;bcd^{E1}	Generated here by Saunders lab
Sc-FV-msGFP2 nosEPr > Sc-FV-msGFP2	Gift from Mounia Lagha (56)
Mutations and RNAis	
endos 1 P{w^{k}}; endos^{1} /TM3, Sb	Gift from Hélène Rangone (79)
endos EY01103 P{w^{k}}; endos^{EY01103} /TM3, Sb	Gift from Hélène Rangone (79)
endos EY01105 P{w^{k}}; endos^{EY01105}/TM3, Sb	Gift from Hélène Rangone (79)

539 **Table S1:** Summary of the *Drosophila* lines used in this work.

540 **Reagents**

Reagent	Supplier/ provider	Catalogue number	Concentration used
Antibodies			
GFP Booster Alexa 488	Chromotek	gb2AF488-100	1:1000 in 0.1% PBST
Rabbit GCN4 Antibody (C11L34) - Chimeric	Novus Biologicals	NBP2-81274SS	1:200 in 0.1% PBST
Goat anti-Rabbit Cy3	Thermofisher Scientific	A10520	1:200 in 0.1% PBST
Goat anti-Rabbit Alexa Flour 647	Thermofisher Scientific	A21245	
Buffers, chemicals, and pharmacological treatments			
Schneider's Insect Media (SIM)	Gibco	21720024	1 X
Activation Buffer (AB)	Made in house: 3.3 mM NaH_2PO_4, 16.6 mM KH_2PO_4, 10mM NaCl, 50 mM KCl, 5% polyethylene glycol (PEG) 8000, 2mM $CaCl_2$, brought to pH 6.4 with a 1:5 ratio of NaOH:KOH (260 mOsm) (Mahowald, Goralski and Caulton, 1983)	-	1 X
Dulbecco's Phosphate Buffered Saline (without $CaCl_2$)	Sigma Aldrich	D8537	1X
1,6 Hexeandiol (1,6-HD)	Sigma Aldrich	240117	5% in Schneider's Insect Medium or 1x PBS

2,5 Hexeandiol (2,5-HD)	Sigma Aldrich	H11904	5% in Schneider's Insect Medium or 1x PBS
Sodium Chloride (NaCl)	Sigma Aldrich	S9888	400 mM in H_2O
NS8593	Sigma Aldrich	492031	Stock: 100 mM in ethanol Final concentration: 100 µM in Schneiders Insect Medium or Activation Buffer (58)
Household Bleach	ESPO	200-300-0011/1	50% in H_2O
Paraformaldehyde	Thermofisher Scientific	J19943-K2	4% in PBS
Methanol	32213	Sigma Aldrich	1 x
Heptane	Thermofisher Scientific	H/0106/PB17	1 x
Triton™ X-100	Sigma Aldrich	X100	0.2% in PBS
Polyoxyethylenesorbitan Monolaurate (Tween-20)	Sigma Aldrich	P1379	0.1% in PBS
De-ionised Formamide	Sigma Aldrich	S4117	10%-30% in various FISH buffer solutions
20 X SCC	Sigma Aldrich	S6639	2X-5X SCC in various FISH buffer solutions
Dextran sulphate	Sigma Aldrich	D6001	10% in various FISH buffer solution
'Wash Buffer A' for Stellaris smFISH	LG Biosearch Technologies	Cat# SMF-WA1-60	20% in de-ionised Formamide and nuclease free H_2O
'Hybridisation Buffer' for Stellaris smFISH	LG Biosearch Technologies	Cat# SMF-HB1-10	90% with de-ionised Formamide
Hybridisation buffer for ImmunoFISH	Made in house (10% Formamide, 2xSSC, Ecoli tRNA (0.36mg/ml), VRC (2mM), 5% Dextran sulphate, ultra pure BSA(0.25mg/ml), stellaris probes, Primary antibody (1:500)		
Tris EDTA (TE) Buffer	Made in house (10 mM Tris-HCl, 1 mM EDTA, pH 8.0)	-	1 x
Slowfade Diamond Antifade Mountant with DAPI	Thermofisher Scientific	S36934	1 X
Oligonucleotides			
(1) Custom Stellaris FISH Probes for the 3'UTR of *bcd* RNA labelled with a Quasar 570 (2) Bcd coding region Quasar 670 (3) 32xSunTag Quasar 570	Stellaris	(See table 2.3 for list of smFISH probes)	Stock: 12.5 µM in TE buffer Final Concentration: 50 nM in 0.25 ml Hybridization buffer
Software and Algorithms			
Image J	Schneider et al., 2012	https://imagej.nih.gov/ij/	
R Studio/ R Software	R Studio Team 2024	http://www.rstudio.com/	
Graphpad Prism			
Other			
Standard Cornmeal Starch Agar FlyFood	Made in house by the Fly Facility, Department of	N/A	N/A

	Genetics, University of Cambridge		
Olympus FV3000 Confocal Laser Scanning Microscope	Olympus	FV3000	N/A

541 **Table S2:** Summary of reagents and tools used in this work.

smFISH probes
5'-GAAACTCTCTAACACGCCTC-3'
5'-ACAGTGGTTAACCTAAAGCT-3'
5'-TGGTATTTGTACAATCAGGA-3'
5'-CTTTCTACGCGTAGATATCT-3'
5'-ACGGATCTTAGGACTAGACC-3'
5'-AAACTTCCCTGGGAACCATT-3'
5'-CTGCTGACTAGGCTAGTACA-3'
5'-GATATGCACTGGAATCCGTG-3'
5'-GAGTTAACTGGAGTATCACT-3'
5'-AGCGTATTGCAGGGAAAGTA-3'
5'-CACCCAGATACATCTAAGGC-3'
5'-CATATTCCCGGGCTTTAGTG-3'
5'-TGGCCTCAAATGTAACTGGT-3'
5'-ACTTTCCATGGAATACGCTT-3'
5'-ATTTCCGAAATGTGGGACGA-3'
5'-AGAAGATTTTCTTGCTGGCT-3'
5'-GTACAGTTTTTAGCTATGTC-3'
5'-ATGAGATTACGCCCAAGAGA-3'
5'-ATGTTCGATCTTTAAGGGTA-3'
5'-ACACTTTGGCATAGCATAGA-3'
5'-GCGCAAATGTTTGATTATGT-3'
5'-TTGCTGACTATTCTTGGTCA-3'
5'-ACAAATGGTCTGCATTGATT-3'
5'-TGATAGTTATTCCGTTTGGC-3'
5'-ATGCTCTTCTTAGTGATGTA-3'
5'-ACTTGAGGCCTAACAGATTG-3'
5'-ACAACATCAAAGGTGCAGCA-3'
5'-ATTTACCCGAGTAGAGTAGT-3'

542 **Table S3:** Custom Stellaris® FISH probes for the 3'UTR of *bcd* RNA (42).

smFISH probes 32XSUNTAG
5'- AGTCCTCTTCTTGAAGAGAG-3'
5'- ATCTCTTACTTCATCGAGCT -3'
5'- AGTCCACTTCTCGAGAATAG -3'
5'- AGAACTTTTACTCCATCGCT -3'
5'- AGACCACTTCTTAACGAGAG -3'
5'- GATAGTGGAGCTCTTGCTTC -3'
5'- CACCTCTTCTTGAAGACAGA -3'

5’- TTAATGGTGGATCTCTTGCT -3’
5’- CCACTTCTTAACGAGAGGTT -3’
5’- GTAAACCTTTTACTTCACCG -3’
5’- GTCGTTCTTGATAGTAGACC -3’
5’- TTCATCGCTCTGACTTTTTT -3’
5’- CGCTTCTTAACGAGAGGTTT -3’
5’- ACCTCTTCTCAATGACTCAT -3’
5’- AATCTTTTACTCCAGCGTTC -3’
5’- TGAGGACAGATTCTTGATGG -3’
5’- GTCTGAATTTTTTCCCTCAC-3’
5’- AGGTTCTTGATGGTAGAGCT-3’
5’- GATCCGACTTTTTTCCAAGA -3’
5’- CGACGAGAGATTTTTGATGG -3’
5’- CTTAATGGTAGACCTCTTGC -3’
5’- CCAAGGCCACTTCTTGATAA -3’
5’- AATGGTAGAGCTCTTACTCC -3’
5’- CTCTTCTCAACGAGAGGTTT -3’
5’- CTTCAACGCGCTGAATTCTT -3’
5’- CTCTTCTTGACAACTCGTTT -3’
5’- ATGGTAGAGCTTTTACTCCA -3’
5’- TGGTAGAGCTCTTACTTCAC -3’
5’- AGAGCTCTTACTTCAACGTG -3’
5’- GTGAACCTTTTGCTTCAACG -3’
5’- TCTTGATAGTGGATCTCTTG -3’
5’- CCATCACCACTTCTTAATGA -3’
5’- CTCTCCTCGATAACTCATTT -3’
5’- TAAATCTCTTACTTCACCGG -3’
5’- GGCCTCTTCTCAACAACAGT -3’
5’- TGATTTCTTTCCAAGTCCTA -3’
5’- CTTCTCGAGGAGAGTTTCTT -3’
5’- CCGCTTCTTAACGAGAGATT -3’
5’- CTAATTTTTTTCCATCACCC -3’
5’- CTCCTTGATGAGAGGTTTTT -3’
5’- TTCGCCACTCCTTAATGAAA -3’
5’- AGTGGAGCTTTTGCTTCAAC -3’
5’- GGCCACTTCTCGATAATAGA -3’
5’- ATCTAATTTTTTCCCATCGC-3’
5’- ACGATTCATTCTTGATGGTG -3’
5’- GAATTTTTTCCCTAGACCTT -3’
5’- TAGTGGAGCTCTTGCTTCAA -3’
5’- TCTCTTACTTCATCGTTCTA -3’

Table S4: Custom Stellaris® FISH probes for the 32xSunTag designed through stellaris probe designer version 4.2

smFISH probes bcd coding region
5’-GGCAGCGGATGATGGTAAAA-3’
5’-AACTGAAGCTGCGGATGTTG-3’
5’-AGGGATTTCGGAATTGTGGC-3’
5’-CGTTCGCTCATCGAAAAGCA-3’
5’-TGTAGTTGTAGTTTATCGCT-3’
5’-CATCTGGTTGGGCAGATACG-3’

5’-GAGGGAAAGACATCTGGCTT-3’
5’-TAAAAGTGGTGCGGGTGCGA-3’
5’-CAGCTCTGCTATTTGAGAGC-3’
5’-TATCGTCCCTGCAGAAAGTG-3’
5’-GCTAGTTTCGCTGACAGATC-3’
5’-ATATCTTCACCTGGGCTGTG-3’
5’-CGACGCCGACGGTTCTTAAA-3’
5’-CTGATCCGATTGGATCTTGT-3’
5’-TTTCATACCCGGCGAGAGAG-3’
5’-AGCTAAGAGTCTGCAAGCTG-3’
5’-GTGACGGAGTCAAAGCGTTG-3’
5’-TGAATGACTCGCTGTAGTGC-3’
5’-TCCATTGTAGTTGTAGTAGG-3’
5’-CATGTGCATGTGACGATTGG-3’
5’-ATTGACATTGGTCGACCCAG-3’
5’-TTGCTTTTGCTGGAAGTCAA-3’
5’-TTGAAGTTGTAGTCGGCCTC-3’
5’-CGATCGCATGTAGTACGAGC-3’
5’-GGTGTTAATGGCTCGTAGAC-3’
5’-AGACTCGGACTTTCGTCATT-3’
5’-AAGATCTGTAGCGTCGTCTT-3’
5’-CTTGTCCAGACCCTTCAAAG-3’
5’-TTCCTGCTAAGGCTCTTATT-3’
5’-AAATGCCGCTCCACGATTTC-3’
5’-GCGAAGGCTTGCCAAATTTG-3’
5’-TGATATTGGTTCGATTCGCC-3’
5’-TTGCATTATCGTATCCATCG-3’
5’-CGTTCCGATGGGGATTATAC-3’
5’-AGTAGGCAAACTGCGAGTTG-3’

Table S5: Custom Stellaris® FISH probes for the bcd coding region designed through stellaris probe designer version 4.2.

Parameter	Description	Value	Reference
$\alpha = \alpha_0 + \alpha_1 \cdot \frac{t^n}{t^n + t_0^n}$	*bcd* degradation rate	$\alpha_0 = 1/180$ *min*$^{-1}$ $\alpha_1 = 1/10$ *min*$^{-1}$ $n = 12,\ t_0 = 120min$	This work and (54)
$\beta \frac{t^m}{t^m + t_1^m}$	*bcd* translation rate	$\beta = 10^{-2}s^{-1}$ $m = 4,\ t_1 = 10min$	Fitted
$D(x) = D_0 + D_1 x/L$	Bcd diffusivity	$D_0 = 4.5\mu m^2 s^{-1}$ $D_1 = 3\mu m^2 s^{-1}$	(45, 80)
L	Embryo length	$500\mu m$	
μ	Bcd degradation rate	$1/35$min^{-1}	(10)
$f(x)$	Initial *bcd* distribution	Figures 4 and S7	This work

Table S6: Model parameters used in Figure 7.

References

1. Turing AM. The chemical basis of morphogenesis. Bulletin of Mathematical Biology. 1952;52:153.
2. Ashe HL, Briscoe J. The interpretation of morphogen gradients. Development. 2006;133:385.
3. Driever W, Nüsslein-Volhard C. A gradient of bicoid protein in Drosophila embryos. Cell. 1988;54:83.
4. Gregor T, Tank DW, Wieschaus EF, Bialek W. Probing the limits to positional information. Cell. 2007;130:153.
5. Rivera-Pomar R, Lu X, Perrimon N, Taubert H, Jäckle H. Activation of posterior gap gene expression in the Drosophila blastoderm. Nature. 1995;376:253.
6. Struhl G, Struhl K, Macdonald PM. The gradient morphogen bicoid is a concentration-dependent transcriptional activator. Cell. 1989;57:1259.
7. Gregor T, Wieschaus EF, McGregor AP, Bialek W, Tank DW. Stability and nuclear dynamics of the bicoid morphogen gradient. Cell. 2007;130:141.
8. Houchmandzadeh B, Wieschaus E, Leibler S. Establishment of developmental precision and proportions in the early Drosophila embryo. Nature. 2002;415:798.
9. Wartlick O, Kicheva A, Gonzalez-Gaitan M. Morphogen gradient formation. Cold Spring Harb Perspect Biol. 2009;1:a001255.
10. Durrieu L, Kirrmaier D, Schneidt T, Kats I, Raghavan S, Hufnagel L, et al. Bicoid gradient formation mechanism and dynamics revealed by protein lifetime analysis. Mol Syst Biol. 2018;14:e8355.
11. Huang A, Saunders TE. A matter of time: Formation and interpretation of the Bicoid morphogen gradient. Curr Top Dev Biol. 2020;137:79.
12. Spirov A, Fahmy K, Schneider M, Frei E, Noll M, Baumgartner S. Formation of the bicoid morphogen gradient: an mRNA gradient dictates the protein gradient. Development. 2009;136:605.
13. Ali-Murthy Z, Kornberg TB. Bicoid gradient formation and function in the Drosophila pre-syncytial blastoderm. Elife. 2016;5:e13222.
14. Coppey M, Berezhkovskii AM, Kim Y, Boettiger AN, Shvartsman SY. Modeling the bicoid gradient: diffusion and reversible nuclear trapping of a stable protein. Dev Biol. 2007;312:623.
15. Grimm O, Coppey M, Wieschaus E. Modelling the Bicoid gradient. Development. 2010;137:2253.
16. Lucas T, Ferraro T, Roelens B, De Las Heras Chanes J, Walczak AM, Coppey M, et al. Live imaging of bicoid-dependent transcription in Drosophila embryos. Curr Biol. 2013;23:2135.
17. Bergmann S, Sandler O, Sberro H, Shnider S, Schejter E, Shilo BZ, et al. Pre-steady-state decoding of the Bicoid morphogen gradient. PLoS Biol. 2007;5:e46.
18. Johnston DS, Driever W, Berleth T, Richstein S, Nüsslein-Volhard C. Multiple steps in the localization of bicoid RNA to the anterior pole of the Drosophila oocyte. Development. 1989;107(Supplement):13.
19. St Johnston D, Nüsslein-Volhard C. The origin of pattern and polarity in the Drosophila embryo. Cell. 1992;68:201.
20. Weil TT, Forrest KM, Gavis ER. Localization of bicoid mRNA in late oocytes is maintained by continual active transport. Dev Cell. 2006;11:251.

21. Weil TT, Parton R, Davis I, Gavis ER. Changes in bicoid mRNA Anchoring Highlight Conserved Mechanisms during the Oocyte-to-Embryo Transition. Current Biology. 2008;18:1055.
22. Kronja I, Yuan B, Eichhorn SW, Dzeyk K, Krijgsveld J, Bartel DP, et al. Widespread changes in the posttranscriptional landscape at the Drosophila oocyte-to-embryo transition. Cell Rep. 2014;7:1495.
23. Kronja I, Whitfield ZJ, Yuan B, Dzeyk K, Kirkpatrick J, Krijgsveld J, et al. Quantitative proteomics reveals the dynamics of protein changes during Drosophila oocyte maturation and the oocyte-to-embryo transition. Proc Natl Acad Sci U S A. 2014;111:16023.
24. Eichhorn SW, Subtelny AO, Kronja I, Kwasnieski JC, Orr-Weaver TL, Bartel DP. mRNA poly(A)-tail changes specified by deadenylation broadly reshape translation in Drosophila oocytes and early embryos. Elife. 2016;5:e16955.
25. Aviles-Pagan EE, Orr-Weaver TL. Activating embryonic development in Drosophila. Semin Cell Dev Biol. 2018;84:100.
26. Weil TT, Parton RM, Herpers B, Soetaert J, Veenendaal T, Xanthakis D, et al. Drosophila patterning is established by differential association of mRNAs with P bodies. Nat Cell Biol. 2012;14:1305.
27. Sankaranarayanan M, Emenecker RJ, Wilby EL, Jahnel M, Trussina I, Wayland M, et al. Adaptable P body physical states differentially regulate bicoid mRNA storage during early Drosophila development. Dev Cell. 2021;56:2886
28. Hubstenberger A, Courel M, Benard M, Souquere S, Ernoult-Lange M, Chouaib R, et al. P-Body Purification Reveals the Condensation of Repressed mRNA Regulons. Mol Cell. 2017;68:144.
29. Standart N, Weil D. P-bodies: cytosolic droplets for coordinated mRNA storage. Trends in Genetics. 2018;34:612.
30. Riggs CL, Kedersha N, Ivanov P, Anderson P. Mammalian stress granules and P bodies at a glance. J Cell Sci. 2020;133.
31. Xing W, Muhlrad D, Parker R, Rosen MK. A quantitative inventory of yeast P body proteins reveals principles of composition and specificity. Elife. 2020;9:e56525.
32. Luo Y, Na Z, Slavoff SA. P-Bodies: Composition, Properties, and Functions. Biochemistry. 2018;57:2424.
33. Bose M, Lampe M, Mahamid J, Ephrussi A. Liquid-to-solid phase transition of oskar ribonucleoprotein granules is essential for their function in Drosophila embryonic development. Cell. 2022;185:1308.
34. Buddika K, Huang YT, Ariyapala IS, Butrum-Griffith A, Norrell SA, O'Connor AM, et al. Coordinated repression of pro-differentiation genes via P-bodies and transcription maintains Drosophila intestinal stem cell identity. Curr Biol. 2022;32:386.
35. Pushpalatha KV, Solyga M, Nakamura A, Besse F. RNP components condense into repressive RNP granules in the aging brain. Nat Commun. 2022;13:2782.
36. Chen R, Stainier W, Dufourt J, Lagha M, Lehmann R. Direct observation of translational activation by a ribonucleoprotein granule. Nature Cell Biology. 2024;26:1322.
37. Ramat A, Haidar A, Garret C, Simonelig M. Spatial organization of translation and translational repression in two phases of germ granules. Nature Communications. 2024;15:8020.

38. Parker R, Sheth U. P bodies and the control of mRNA translation and degradation. Mol Cell. 2007;25:635.
39. Davidson A, Parton RM, Rabouille C, Weil TT, Davis I. Localized Translation of gurken/TGF-alpha mRNA during Axis Specification Is Controlled by Access to Orb/CPEB on Processing Bodies. Cell Rep. 2016;14:2451.
40. Wang M, Ly M, Lugowski A, Laver JD, Lipshitz HD, Smibert CA, et al. ME31B globally represses maternal mRNAs by two distinct mechanisms during the Drosophila maternal-to-zygotic transition. Elife. 2017;6:e27891.
41. St Johnston D. Polarity and axis formation in the Drosophila female germ line. Curr Top Dev Biol. 2023;154:73.
42. Trovisco V, Belaya K, Nashchekin D, Irion U, Sirinakis G, Butler R, et al. bicoid mRNA localises to the Drosophila oocyte anterior by random Dynein-mediated transport and anchoring. Elife. 2016;5:e17537.
43. Weil TT, Xanthakis D, Parton R, Dobbie I, Rabouille C, Gavis ER, et al. Distinguishing direct from indirect roles for bicoid mRNA localization factors. Development. 2010;137:169.
44. Porcher A, Abu-Arish A, Huart S, Roelens B, Fradin C, Dostatni N. The time to measure positional information: maternal hunchback is required for the synchrony of the Bicoid transcriptional response at the onset of zygotic transcription. Development. 2010;137:2795.
45. Athilingam T, Nelanuthala AVS, Breen C, Karedla N, Fritzsche M, Wohland T, et al. Long-range formation of the Bicoid gradient requires multiple dynamic modes that spatially vary across the embryo. Development. 2024;151:dev202128.
46. Tanenbaum ME, Gilbert LA, Qi LS, Weissman JS, Vale RD. A protein-tagging system for signal amplification in gene expression and fluorescence imaging. Cell. 2014;159:635.
47. Pichon X, Bastide A, Safieddine A, Chouaib R, Samacoits A, Basyuk E, et al. Visualization of single endogenous polysomes reveals the dynamics of translation in live human cells. J Cell Biol. 2016;214:769.
48. Wang C, Han B, Zhou R, Zhuang X. Real-Time Imaging of Translation on Single mRNA Transcripts in Live Cells. Cell. 2016;165:990.
49. Wu B, Eliscovich C, Yoon YJ, Singer RH. Translation dynamics of single mRNAs in live cells and neurons. Science. 2016;352:1430.
50. Yan X, Hoek TA, Vale RD, Tanenbaum ME. Dynamics of Translation of Single mRNA Molecules In Vivo. Cell. 2016;165:976.
51. Dufourt J, Bellec M, Trullo A, Dejean M, De Rossi S, Favard C, et al. Imaging translation dynamics in live embryos reveals spatial heterogeneities. Science. 2021;372:840.
52. Vinter DJ, Hoppe C, Minchington TG, Sutcliffe C, Ashe HL. Dynamics of hunchback translation in real-time and at single-mRNA resolution in the Drosophila embryo. Development. 2021;148:dev196121.
53. Blake LA, De La Cruz A, Wu B. Imaging spatiotemporal translation regulation in vivo. Seminars in Cell & Developmental Biology. 2024;154:155.
54. Little SC, Tkacik G, Kneeland TB, Wieschaus EF, Gregor T. The formation of the Bicoid morphogen gradient requires protein movement from anteriorly localized mRNA. PLoS Biol. 2011;9:e1000596.

686 55. York-Andersen AH, Parton RM, Bi CJ, Bromley CL, Davis I, Weil TT. A single and
687 rapid calcium wave at egg activation in Drosophila. Biol Open. 2015;4:553.
688 56. Bellec M, Chen R, Dhayni J, Trullo A, Avinens D, Karaki H, et al. Boosting the
689 toolbox for live imaging of translation. RNA. 2024;30:1374.
690 57. Mahowald AP, Goralski TJ, Caulton JH. In vitro activation of Drosophila eggs.
691 Developmental biology. 1983;98:437.
692 58. Hu Q, Wolfner MF. The Drosophila Trpm channel mediates calcium influx during
693 egg activation. Proc Natl Acad Sci U S A. 2019;116:18994.
694 59. Bose M, Rankovic B, Mahamid J, Ephrussi A. An architectural role of specific
695 RNA-RNA interactions in oskar granules. Nat Cell Biol. 2024 *in press*.
696 60. Alberti S, Gladfelter A, Mittag T. Considerations and Challenges in Studying
697 Liquid-Liquid Phase Separation and Biomolecular Condensates. Cell. 2019;176:419.
698 61. McSwiggen DT, Mir M, Darzacq X, Tjian R. Evaluating phase separation in live
699 cells: diagnosis, caveats, and functional consequences. Genes Dev. 2019;33:1619.
700 62. Gao Y, Li X, Li P, Lin Y. A brief guideline for studies of phase-separated
701 biomolecular condensates. Nature Chemical Biology. 2022;18:1307.
702 63. Horner VL, Wolfner MF. Mechanical stimulation by osmotic and hydrostatic
703 pressure activates Drosophila oocytes in vitro in a calcium-dependent manner. Dev
704 Biol. 2008;316:100.
705 64. Von Stetina JR, Tranguch S, Dey SK, Lee LA, Cha B, Drummond-Barbosa D.
706 alpha-Endosulfine is a conserved protein required for oocyte meiotic maturation in
707 Drosophila. Development. 2008;135:3697.
708 65. Rangone H, Bond L, Weil TT, Glover DM. Greatwall-Endos-PP2A/B55(Twins)
709 network regulates translation and stability of maternal transcripts in the Drosophila
710 oocyte-to-embryo transition. Open Biol. 2024;14:240065.
711 66. Surdej P, Jacobs-Lorena M. Developmental regulation of bicoid mRNA stability is
712 mediated by the first 43 nucleotides of the 3' untranslated region. Molecular and
713 cellular biology. 1998;18:2892.
714 67. Wang C-Y, Wang Y-T, Hsiao W-Y, Wang S-W. Involvement of fission yeast Pdc2 in
715 RNA degradation and P-body function. Rna. 2017;23:493.
716 68. Eichler CE, Hakes AC, Hull B, Gavis ER. Compartmentalized oskar degradation in
717 the germ plasm safeguards germline development. Elife. 2020;9:e49988.
718 69. Forbes Beadle L, Love JC, Shapovalova Y, Artemev A, Rattray M, Ashe HL.
719 Combined modelling of mRNA decay dynamics and single-molecule imaging in the
720 Drosophila embryo uncovers a role for P-bodies in 5' to 3' degradation. PLoS Biol.
721 2023;21:e3001956.
722 70. He F, Saunders TE, Wen Y, Cheung D, Jiao R, ten Wolde PR, et al. Shaping a
723 morphogen gradient for positional precision. Biophys J. 2010;99:697.
724 71. Baumgartner S. Seeing is believing: the Bicoid protein reveals its path. Hereditas.
725 2018;155:28.
726 72. Shlemov A, Alexandrov T, Golyandina N, Holloway D, Baumgartner S, Spirov AV.
727 Quantification reveals early dynamics in Drosophila maternal gradients. PLoS One.
728 2021;16:e0244701.
729 73. Kramer S. Simultaneous detection of mRNA transcription and decay
730 intermediates by dual colour single mRNA FISH on subcellular resolution. Nucleic Acids
731 Res. 2017;45:e49.

732 74. Patel PH, Barbee SA, Blankenship JT. GW-Bodies and P-Bodies Constitute Two
733 Separate Pools of Sequestered Non-Translating RNAs. PLoS One. 2016;11:e0150291.
734 75. Weil TT, Parton RM, Davis I. Preparing individual Drosophila egg chambers for live
735 imaging. J Vis Exp. 2012;60:3679.
736 76. Abbaszadeh EK, Gavis ER. Fixed and live visualization of RNAs in Drosophila
737 oocytes and embryos. Methods. 2016;98:34.
738 77. Bolte S, Cordelieres FP. A guided tour into subcellular colocalization analysis in
739 light microscopy. J Microsc. 2006;224:213.
740 78. Buszczak M, Paterno S, Lighthouse D, Bachman J, Planck J, Owen S, et al. The
741 carnegie protein trap library: a versatile tool for Drosophila developmental studies.
742 Genetics. 2007;175:1505.
743 79. Rangone H, Wegel E, Gatt MK, Yeung E, Flowers A, Debski J, et al. Suppression of
744 scant identifies Endos as a substrate of greatwall kinase and a negative regulator of
745 protein phosphatase 2A in mitosis. PLoS Genet. 2011;7:e1002225.
746 80. Liu F, Morrison AH, Gregor T. Dynamic interpretation of maternal inputs by the
747 Drosophila segmentation gene network. Proceedings of the National Academy of
748 Sciences. 2013;110:6724.
749

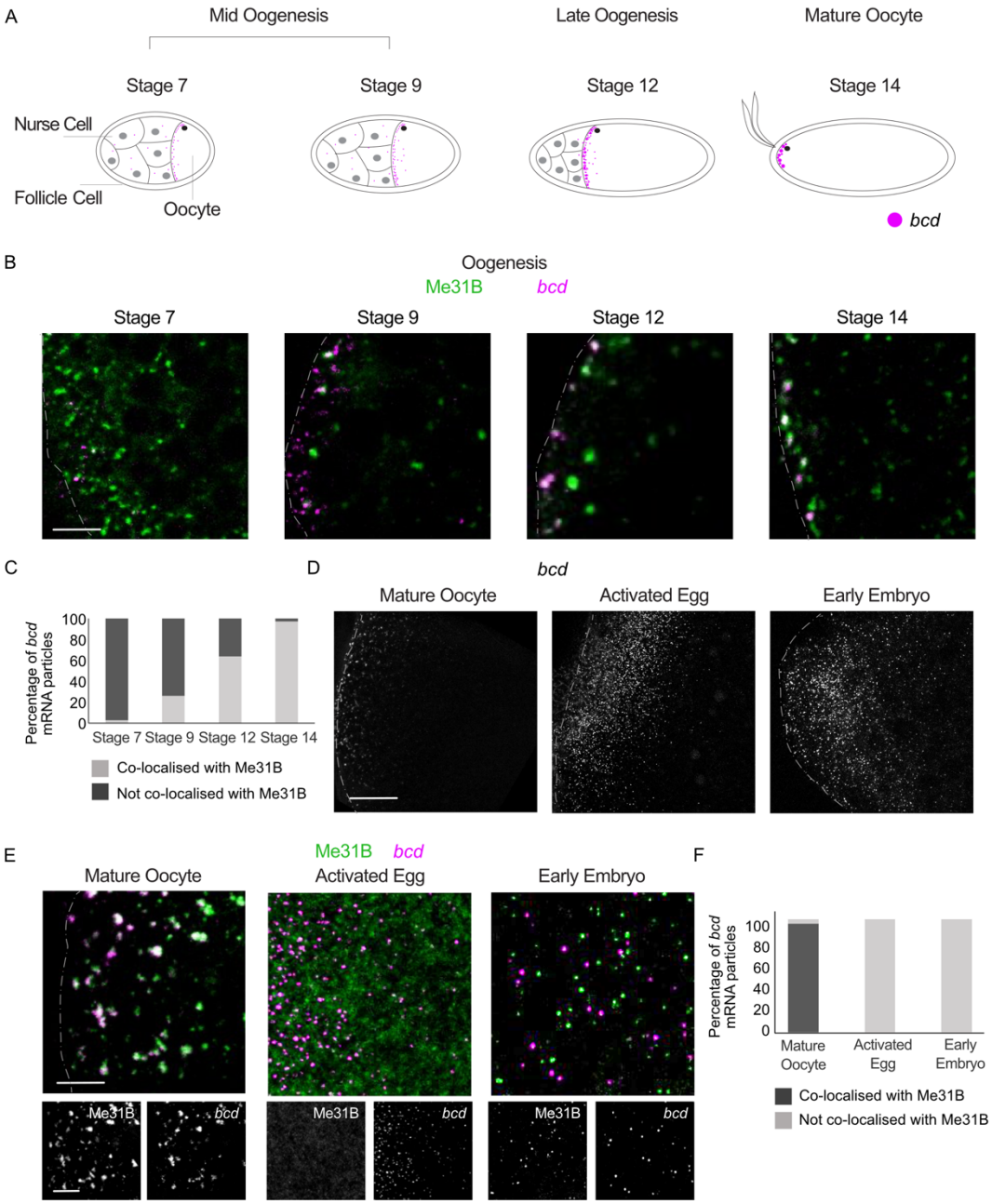

Figure 1: *bcd* mRNA association with P bodies is dynamic over developmental time

A: Schematic illustrating *Drosophila* oogenesis from mid oogenesis to the mature oocyte. *bcd* (magenta) increasingly localises to the anterior margin through these stages.

B: Fixed single plane images showing Me31B::GFP (green, anti-GFP-nanobody) and *bcd* (magenta, smFISH) throughout oogenesis.

C: Quantification of the co-localisation between *bcd* particles and Me31B::GFP particles throughout oogenesis.

D: Fixed 10 µm Z-stack images showing *bcd* (smFISH) at the anterior of the mature oocyte, *in vitro* activated egg, and in the anterior pole of the embryo 30-minute post fertilisation.
E: Fixed 10 µm Z-stack images showing Me31B::GFP (green, anti-GFP-nanobody) and *bcd* (magenta, smFISH) in mature oocyte, *in vitro* activated egg, and anterior pole of embryo 30-minute post fertilisation. Single channel images are shown for Me31B and *bcd*.

F: Quantification of the co-localisation between *bcd* particles and Me31B::GFP particles in mature oocytes, *in vitro* activated eggs, and embryos 30-minute post fertilisation.

Scale bars: B, E = 5 µm; D = 20 µm

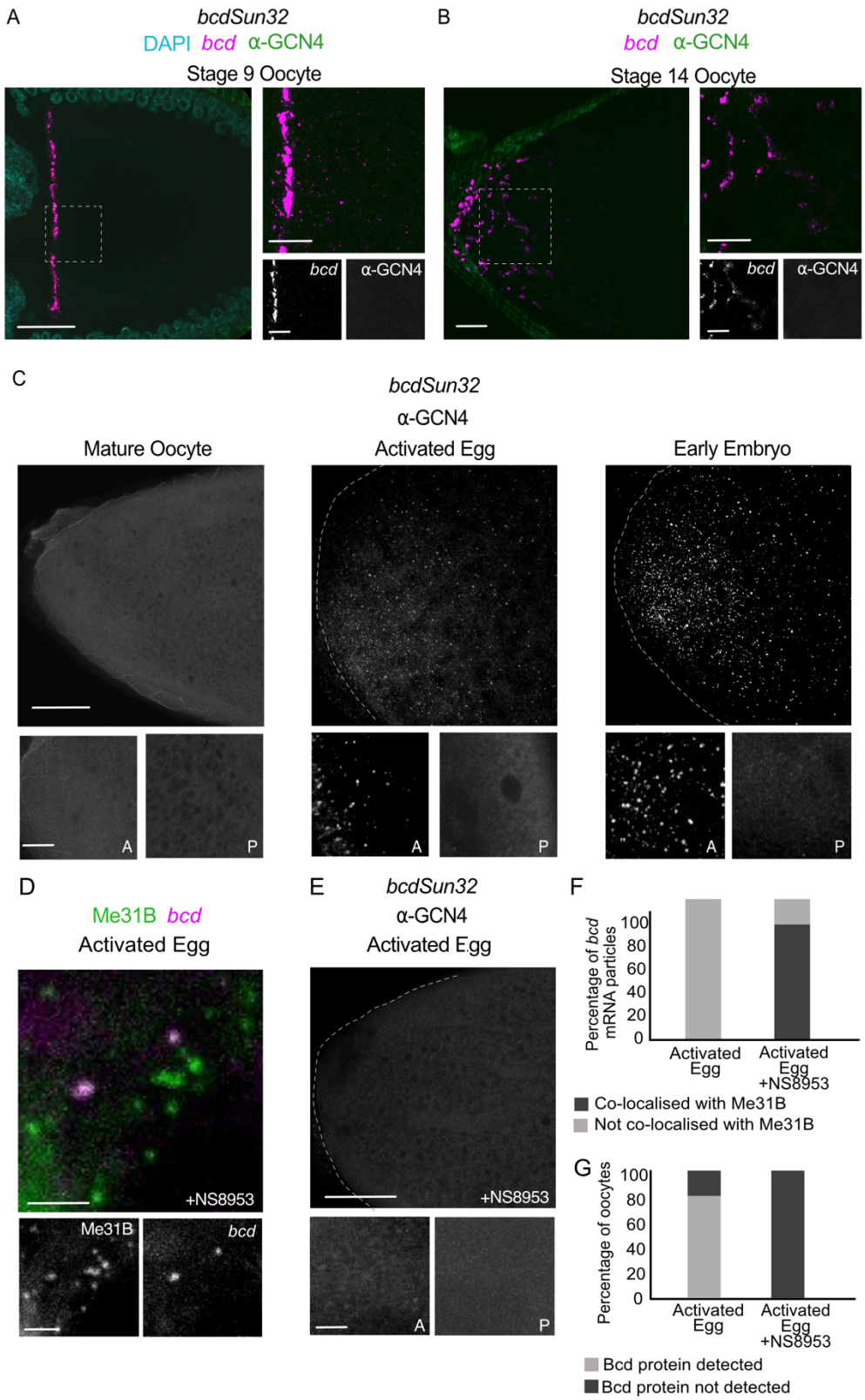

Figure 2: *bcdSun32* reporter enables visualisation of *bcd* mRNA translation

A-B: Fixed 5-10 µm Z-stack images showing *bcdSun32* labelled *bcd* (magenta, smFISH) localising to the anterior margin of stage 9 and 14 oocytes. SunTag labelled Bcd (BcdSun32) protein (green, anti-GCN4) not detected in stage 9 or 14 oocytes (green, anti-GCN4).

C: Fixed 10 µm Z-stack images showing BcdSun32 protein (anti-GCN4) at the anterior of a mature oocyte, *in vitro* activated mature oocyte, and embryo 30-minute post fertilisation. Zoomed images of the mature oocyte show that Bcd protein is not detected at the anterior pole or posterior pole of the same mature oocyte. However, zoomed images of the *in vitro* activated mature oocyte and embryo 30-minute post fertilisation show that BcdSun32 protein was detected at the anterior pole and not the posterior pole of the same activated oocyte.

D: Fixed single plane images showing Me31B::GFP (green, anti-GFP-nanobody) and *bcd* (magenta, smFISH) at the anterior of *in vitro* activated oocyte incubated with NS8953, a calcium channel blocker. Single channel images are shown for Me31B and *bcd*.

E: Fixed 10 µm Z-stack images showing the overall distribution of BcdSun32 protein at the anterior of an *in vitro* activated oocyte incubated with NS8953. Zoomed images show that BcdSun32 protein (anti-GCN4) is not detected at the anterior pole or the posterior pole of the same activated oocyte.

F: Quantification of the co-localisation between *bcd* particles and Me31B::GFP particles in *in vitro* activated oocytes incubated with 10 µm NS8953 for 20 minutes compared to *in vitro* activated oocytes. N = 3 oocytes.

G: Quantification of the number of oocytes that displayed *bcd* translation as measured by the presence of BcdSun32 protein at the anterior of the oocyte, but not the posterior, in *in vitro* activated oocytes incubated with 10 µm NS8953 for 20 minutes compared to in vitro activated oocytes. N = 30 oocytes.

Scale Bars: A-B = 50 µm; A-B (zoom) = 10 µm; C, E = 20 µm; C, E (zoom) = 2 µm; D = 5 µm

A = Anterior; P = Posterior.

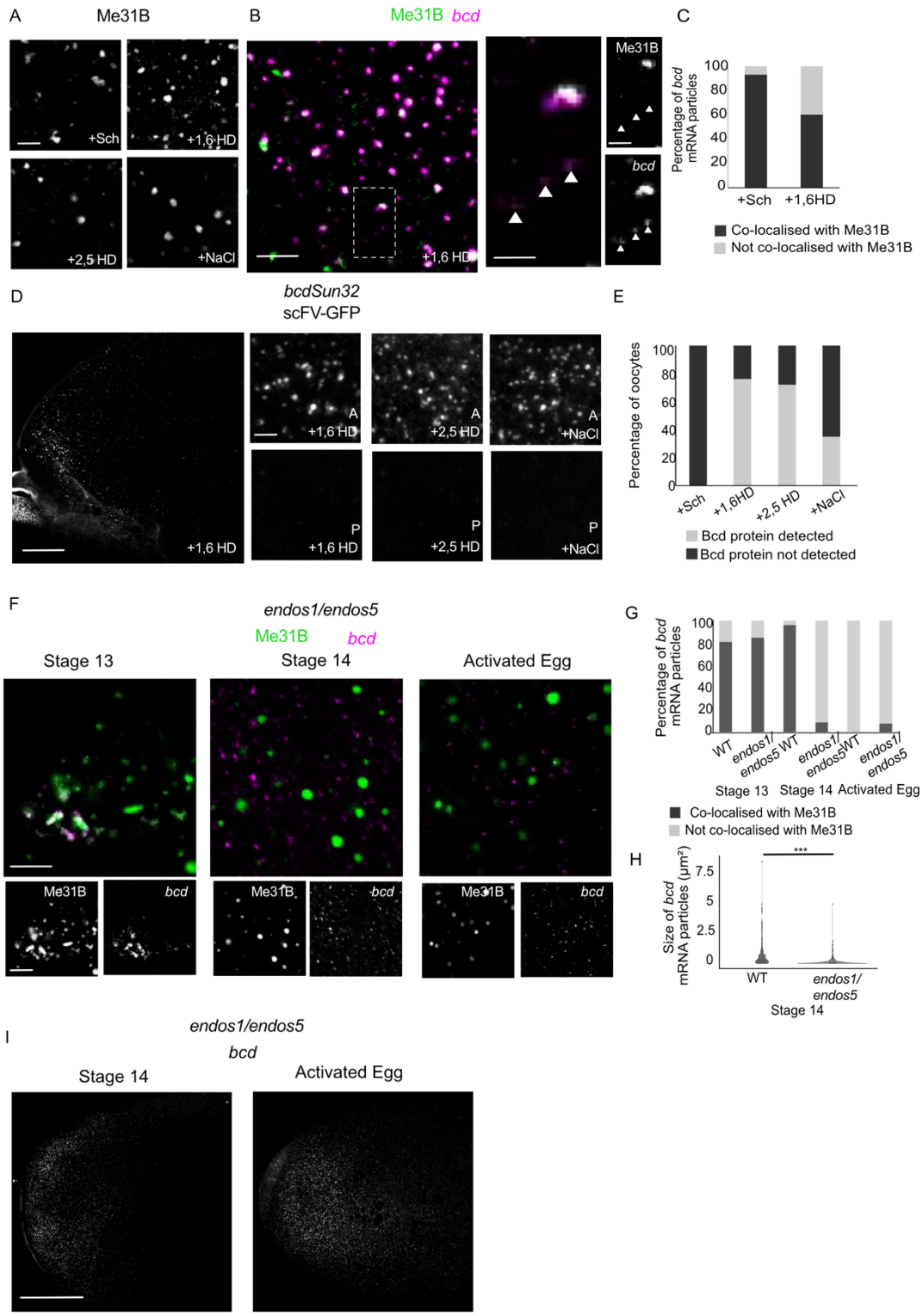

Figure 3: Chemical and genetic manipulation of P bodies can cause *bcd* mRNA misregulation

A: Fixed single plane images showing the distribution of Me31B::GFP (green, anti-GFP-nanobody) in mature oocytes incubated for 20 minutes in Schneider's insect medium (control), 5% 1,6 hexanediol, 5% 2,5 hexanediol, 400 mM NaCl. P bodies become more circular and uniform in size under these experimental conditions (27).

B: Fixed single plane images showing Me31B::GFP (green, anti-GFP-nanobody) and *bcd* (magenta, smFISH) in mature oocytes incubated in 5% 1,6 hexanediol for 20 minutes. The highlighted box is zoomed and shows both merged and single channel images. *bcd* becomes disassociated with P bodies. Arrowheads show *bcd* that no longer co-localises with P-bodies.

C: Quantification of *bcd* particles in mature oocytes incubated in 5% 1,6 hexanediol for 20 minutes compared to oocytes incubated in Schneider's insect medium (control). N = between 6-10 oocytes for each treatment CST *** P<0.001.

D: Fixed 10 µm Z-stack image showing the overall distribution of BcdSun32 protein (scFV-GFP, anti-GFP-nanobody) at the anterior of a mature oocyte incubated in 5% 1,6 hexanediol for 20 minutes. Zoomed images show that BcdSun32 protein is detected at the anterior pole and not at the posterior pole of the same 5% 1,6 hexanediol treated mature oocyte. We observe a similar outcome upon treatment with in 5% 2,5 hexanediol and 400 mM NaCl.

E: Quantification of experiments shown in D. The number of oocytes that displayed Bcd protein at the anterior as measured by the presence of BcdSun32 at the anterior of the oocyte, but not the posterior. N = 30 oocytes for each treatment.

F: Fixed single plane image showing the distribution of Me31B::GFP (green, anti-GFP-nanobody) and *bcd* (magenta, smFISH) in a stage 13 oocyte, stage 14 oocyte and an *in vitro* activated egg in an Endos mutant background.

G: Quantification of the co-localisation between *bcd* particles and Me31B::GFP particles in an Endos mutant background compared to the wildtype in stage 13, stage 14 oocytes, and *in vitro* activated eggs. N = between 6-10 oocytes for each genotype.

H: Quantification of the size of *bcd* particles in Endos mutant background compared to the wildtype in stage 14 oocytes. *bcd* particles in wildtype mature oocytes are significantly larger than in Endos mutant backgrounds. Wilcoxon signed-rank test, *** $p < 0.001$, N = 5 oocytes.

I: Fixed 10 µm Z-stack image showing the overall distribution of *bcd* (magenta, smFISH) at the anterior of the mature oocytes and *in vitro* activated eggs in Endos mutant background. *bcd* appears to be more particulate and diffuse at the anterior compared to wildtype (Figure 1D)

Scale Bars: A, B, F = 5 µm; B (zoom), D = 2 µm; D, I = 20 µm

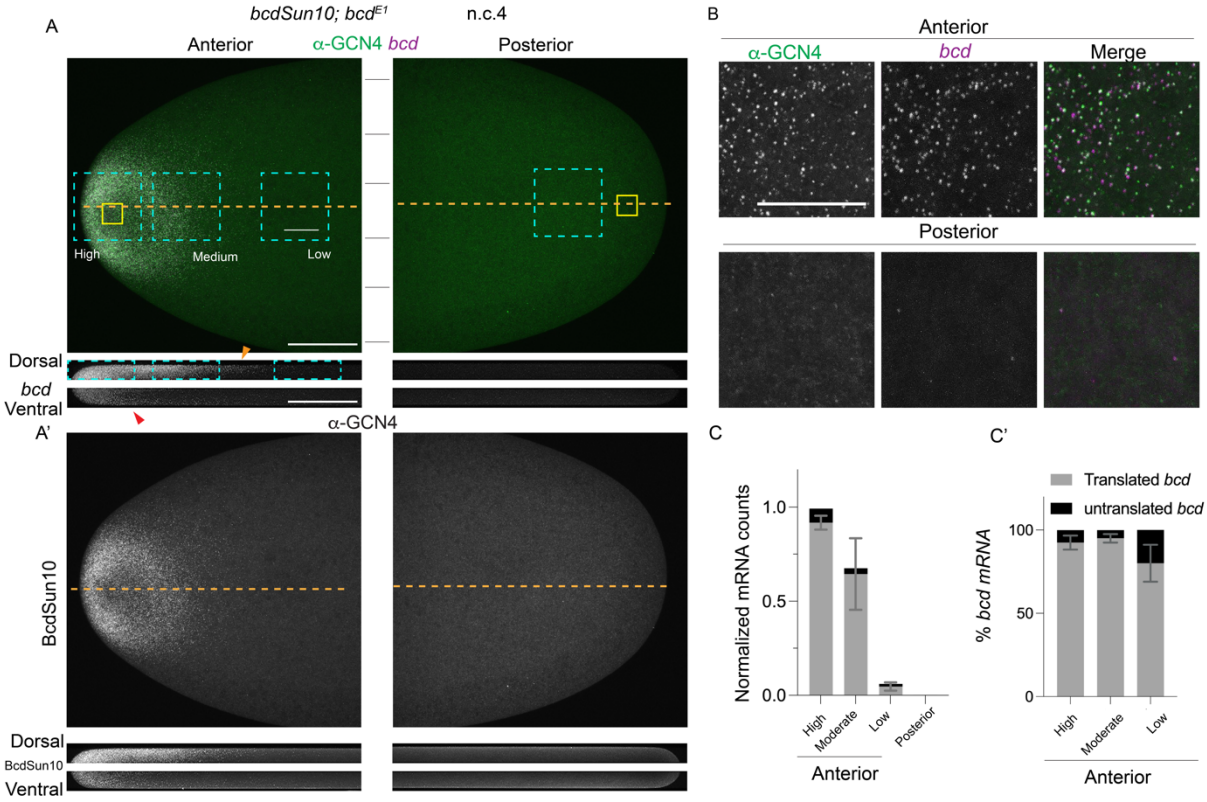

Figure 4: *bcd* mRNA is translated exclusively in the anterior domain of the early *Drosophila* embryo

A-A': Projected Z-stacks of the anterior and posterior domain of n.c. 4 embryo expressing the *bcdSun10* transgene, stained for *bcd* coding region (magenta) and SunTag, anti-GCN4 (green) using Immuno-FISH. The projected cross sections in the bottom panel show the dorsal and ventral surface of the anterior and posterior domains of the embryo. Translating *bcdSun10* is shown in A' along with projected cross sections.

B: Yellow boxes from A are magnified to show colocalisation of SunTag to *bcd*.

C: Normalised *bcd* counts from the cyan boxes in A located at regions of varied mRNA counts across AP-axis. Data normalised to the total mRNA counts from the most anterior region analysed.

C': Percentage of translated and untranslated *bcd* mRNA at different locations (cyan boxes in A) in the anterior and posterior domains (N = 3 embryos) in n.c. 4. Error bars = s.d.

Scale Bars: A, A' = 50 µm; B = 25 µm

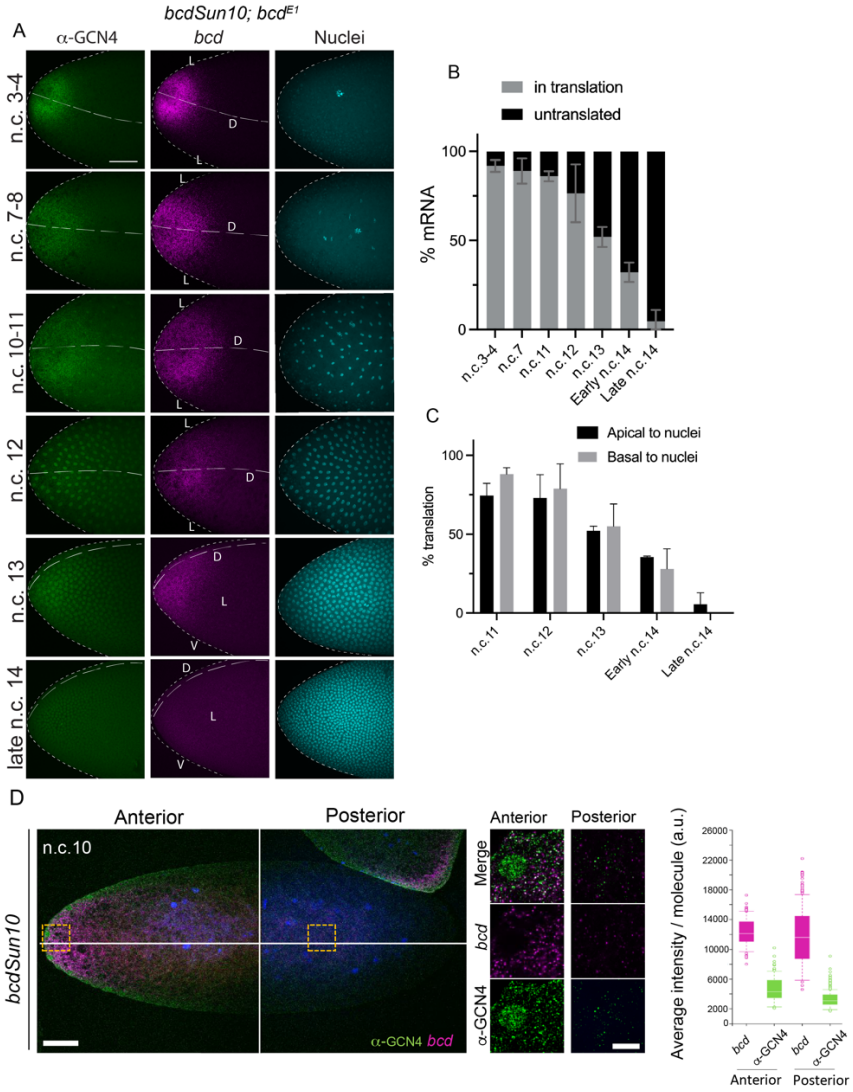

Figure 5: Temporal changes in *bcd* translation from early to late blastoderm

A: *bcdSun10* translation detected through immuno-FISH marked for SunTag translation (anti-GCN4, green) and *bcd* (magenta) from the early to late blastoderm embryo. D = dorsal; V = ventral; V = ventral

B: Percentage of *bcd* undergoing translation at different nuclear cycles. N = 3 embryos in each of the nuclear stages. Error bars = s.d.

C: Percentage of *bcd* translation in either the apical or basal domains in different nuclear cycles. N = 3 embryos in each of the nuclear stages. Error bars = s.d.

D: Projected Z stacks of the anterior and posterior domains embryos expressing *bcdSun10* transgenes. *bcd* reporters and translation spots were detected by Immuno-FISH using Suntag probes and anti-GCN4 shown in magenta and green respectively. Quantification of the single molecule average intensity for *bcd*-reporters FISH and GCN4 immunofluorescence signals in anterior and posterior domains (right panel).

Scale bars: A = 50μm

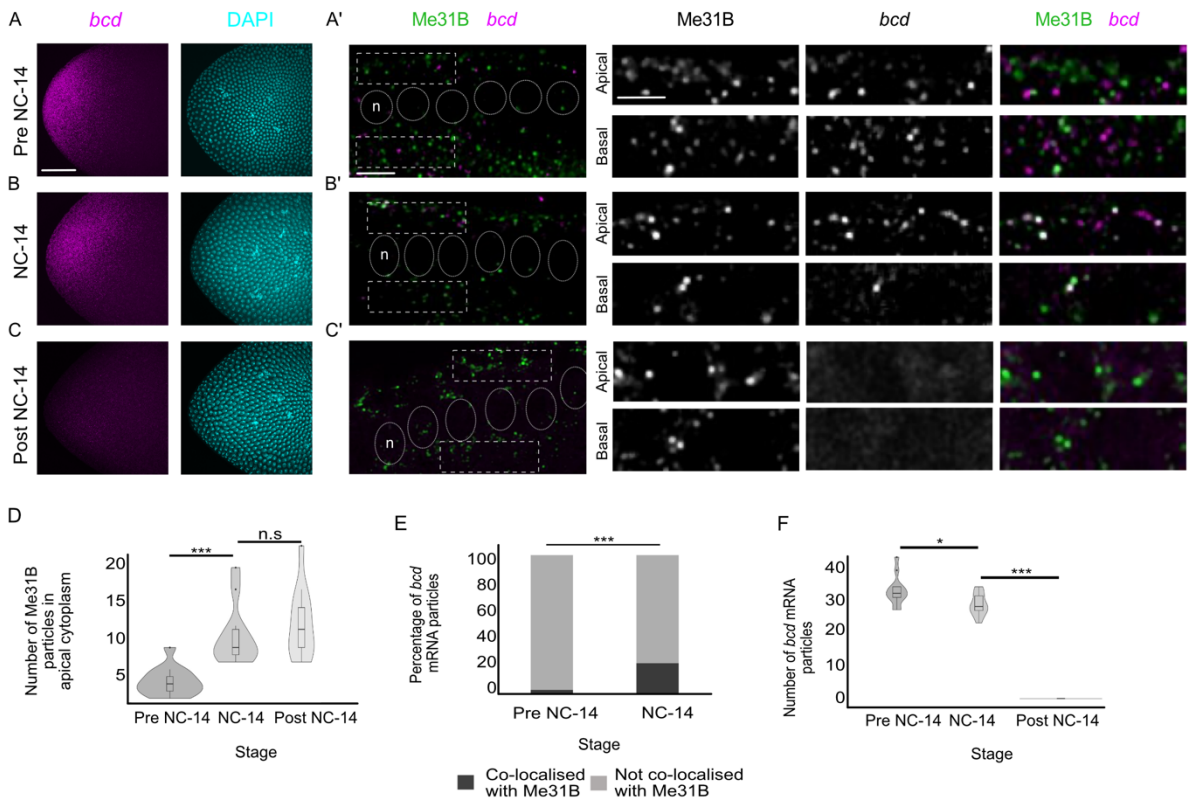

Figure 6: *bcd* re-associates with P bodies in n.c. 14, coinciding with their degradation.

A-C: Fixed projected Z-stack images showing *bcd* (magenta, smFISH) and DAPI (cyan) pre-n.c. 14, n.c. 14, and post-n.c. 14.

A'-C': Fixed single plane images showing Me31B::GFP (green, anti-GFP-nanobody) and *bcd* (magenta, smFISH). (Right) Zoomed regions of the apical side and basal side are shown for Me31B, *bcd*, and merged, respectfully. n = nucleus

D: P body number present in the apical cytoplasm, pre-n.c. 14, n.c. 14, and post-n.c. 14 embryos.

E: Co-localisation between *bcd* and Me31B::GFP particles in the apical cytoplasm of pre-n.c. 14 and n.c. 14 embryos.

F: *bcd* particles present in the apical cytoplasm in pre-n.c. 14, n.c. 14, and post-n.c. 14.

Scale bars: A-C = 50 µm; A'-C' = 10 µm; A'-C' (zoomed) = 5 µm

* $p < 0.05$; *** $p < 10^{-3}$.

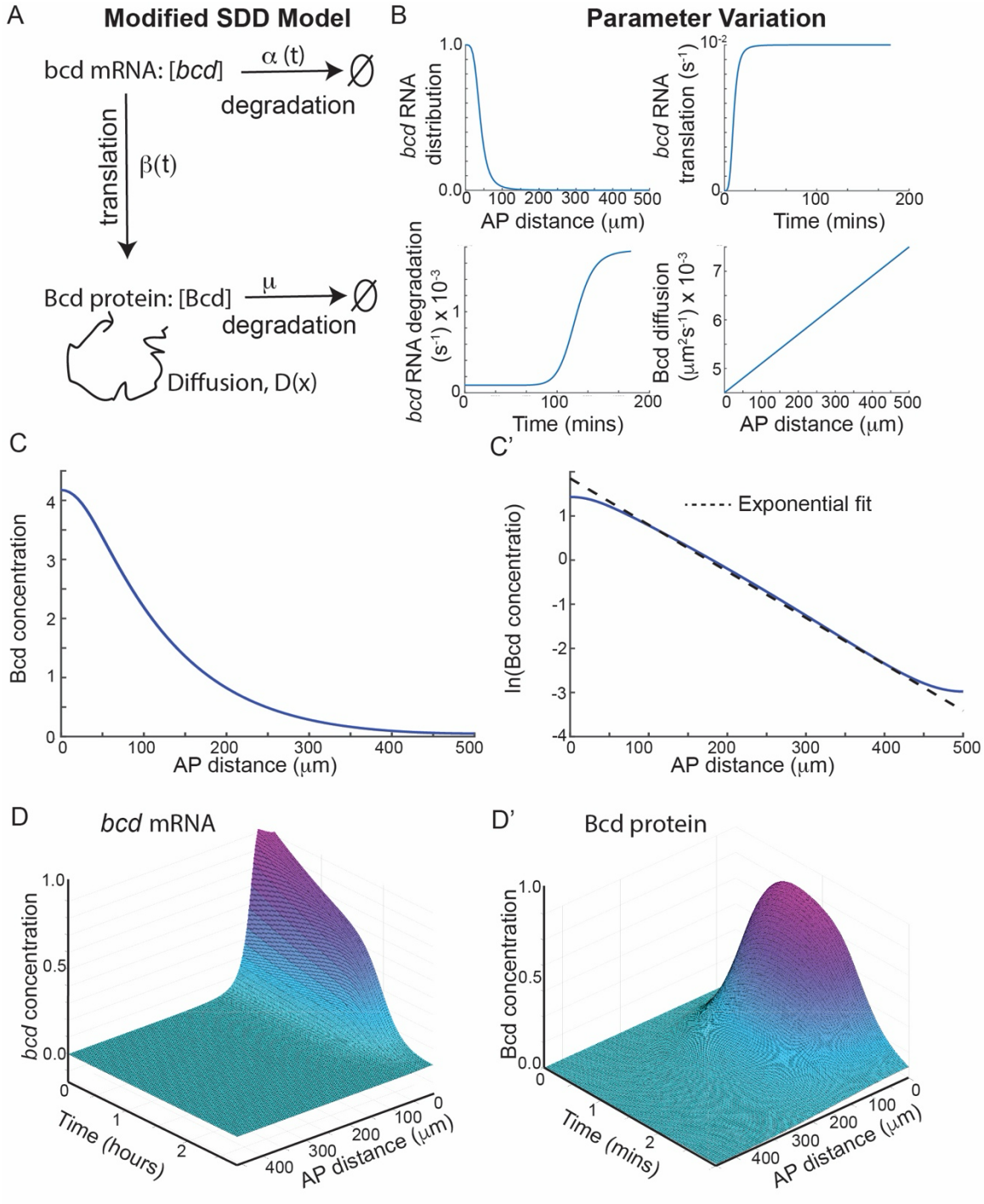

Figure 7: Modified SDD model of Bcd gradient formation

A: Model schematic, outlining parameters defining *bcd* and Bcd production, degradation and movement.

B: Initial conditions (i) and parameter variation (ii-iv) over time or space within the model.

C: Bcd concentration after 120 minutes in the simulation. C': Same as C on log-plot, with an exponential fit shown with the dashed black line. Dashed line has decay length of 85 μm.

D: Normalised concentration in space and time for *bcd* (D) and Bcd protein (D').